Attenuation Coefficient Estimates of Mouse and Rat Chest Wall

Geraldine A. Teotico, Rita J. Miller, Leon A. Frizzell, *Senior Member, IEEE*, James F. Zachary, and William D. O'Brien, Jr., *Fellow, IEEE*

***Abstract*—Attenuation coefficients of intercostal tissues were estimated from chest walls removed postmortem (pm) from 41 6-to-7-week-old female ICR mice and 27 10-to-11-week-old female Sprague-Dawley rats. These values were determined from measurements through the intercostal tissues, from the surface of the skin to the parietal pleura. Mouse chest walls were sealed in plastic wrap and stored at 4°C until evaluated, and rat chest walls were sealed in Glad-Lock® Zipper™ sandwich bags, and stored at −15°C. When evaluated, chest wall storage time ranged between 1 and 2 days pm for mice and between 41 and 110 days pm for rats. All chest walls were allowed to equilibrate to 22°C in a water bath prior to evaluation. For both mouse and rat intercostal tissues, the estimated frequency normalized attenuation coefficient was 1.1 dB/cm-MHz. In order to determine if there was an effect of storage time on estimates of attenuation coefficient, an independent experiment was conducted. The intercostal tissues from six mouse chest walls were evaluated at three time points (1, 22, and 144 days pm), and from six rat chest walls were evaluated at four time points (1, 22, 50, and 125 days pm). There was no difference in the estimated intercostal tissue attenuation coefficient as a function of time postmortem.**

I. Introduction

Several groups have published experimental findings documenting lung hemorrhage (bioeffect) in mice [1]–[9], rats [10], [11], rabbits [6], [8], monkeys [12], and pigs [8], [13], [14] at levels of ultrasound exposure and pulsing conditions consistent with those used for ultrasonography in humans. The authors have conducted more recent studies of ultrasound-induced lung hemorrhage in mice and rats. One of these studies has demonstrated that lung hemorrhage in mice is not produced by inertial cavitation [15]. Another study has examined the thresholds for hemorrhage and superthreshold lesion development in both mice and rats at 2.8 and 5.6 MHz [16].

Although diagnostic ultrasound equipment and ultrasound bioeffect field measurements are made in water, proper in situ estimation of the ultrasound field quantities is required to assist in evaluating mechanisms for the observed effects. There have been very few measurements of the ultrasonic propagation properties of the intercostal tissues (skin, panniculus muscle, subcutaneous adipose tissue [fat], intercostal muscle, and parietal pleura) (Table I). These data are essential to estimate in situ (at the pleural surface) ultrasonic exposure levels in the case of ultrasound-induced lung hemorrhage evaluations [15], [17]. This paper provides the detailed methodology and results for the intercostal tissue (space between the ribs) of adult mouse and rat chest wall attenuation coefficient estimates.

Manuscript received March 17, 2000; accepted September 19, 2000. This work was supported by NIH Grant HL58218 awarded to W. D. O'Brien, Jr. and J. F. Zachary.

G. A. Teotico, R. J. Miller, L. A. Frizzell, and W. D. O'Brien, Jr. are with the Bioacoustics Research Laboratory, Department of Electrical and Computer Engineering, University of Illinois, Urbana, IL 61801 (e-mail: wdo@uiuc.edu).

J. F. Zachary is with the Department of Veterinary Pathobiology, University of Illinois, Urbana, IL 61802.

II. Materials and Methods

Two separate experiments are reported. Experiment 1 estimated the intercostal tissue attenuation coefficient for randomly selected animals that were included in lung hemorrhage studies [15], [16]. Experiment 2 evaluated the effect of storage time on estimates of insertion loss values. The experimental protocol was approved by the campus' Laboratory Animal Care Advisory Committee and satisfied all campus and NIH rules for the humane use of laboratory animals. Animals were housed in an AAALAC-approved animal facility, placed in groups of three or four in polycarbonate cages with beta-chip bedding and wire bar lids, and provided food and water ad libitum.

A. Experiments

1. Experiment 1: Chest walls from 41 6-to-7-week-old 34.3 ± 6.4-g female ICR mice (Harlan Sprague Dawley Laboratories, Indianapolis, IN) and 27 10-to-11-week-old 278 ± 14-g female Sprague-Dawley rats (Harlen Sprague Dawley Laboratories, Indianapolis, IN) were obtained at random from an ongoing ultrasound-induced lung hemorrhage study [15], [16].

Mice and rats were weighed then anesthetized with ketamine hydrochloride (87.0 mg/kg) and xylazine (13.0 mg/kg) administered intraperitoneally. For each animal, the skin of the left thorax was exposed by removing the hair with an electric clipper, followed by a depilatory agent (Nair® Carter-Wallace, Inc., New York, NY) to maximize sound transmission. Following the ultrasound-induced lung hemorrhage exposure procedure [15], [16], animals were euthanized under anesthesia by cervical dislocation. The thorax was opened via a median sternotomy, and the thickness of each left chest wall between the ribs (skin, panniculus muscle, subcutaneous adipose tissue [fat], intercostal muscle, and parietal pleura) at the point of ex-

0885–3010/$10.00 © 2001 IEEE

TABLE I
SUMMARY OF ULTRASONIC PROPERTIES OF CHEST WALLS
(BLANKS INDICATE THAT DATA WERE NOT REPORTED).

Species	Age	Thickness (mm)	Frequency (MHz)	Measured loss (dB)	Estimated loss or atten. coef.	Reference
Mouse	7 wk		1.1	1.5–5.2		[1] Child *et al.*, 1990
			3.4	2.5–6.9		
Mouse			1.1		1.9 dB	[4] Raeman *et al.*, 1993
Mouse	6-7 wk	2	3 & 6		1 dB/cm-MHz	[8] O'Brien and Zachary, 1997

posure was measured using a Mitutoyo Digimatic Caliper (Mitutoyo Corp., Kawasaki, Kanagawa, Japan) (accuracy of 10 μm). (Note: This is not the thickness used to estimate attenuation coefficient in this contribution. In general, this chest wall thickness measurement was about 1 mm greater than reported below. It was not possible to make a precise thickness measurement of only the intercostal tissue space because of the closeness of the ribs.) The sternotomy incision was continued along the ventral midline, with a curvilinear incision caudal to the last rib, which extended to the spinal column. This incision was then continued with a dorsal incision off midline, and the chest wall was separated from the spinal column. A curvilinear incision was made cranial to the first rib, connecting to the median sternotomy. Immediately following removal, the mouse and rat chest walls were placed in a 0.9% sodium chloride solution then wrapped in plastic wrap or sealed in Glad-Lock® Zipper™ sandwich bags, respectively. The mouse chest wall samples were stored for 1-2 days in a refrigerator (4°C) prior to insertion loss measurements. Rat chest wall samples were stored for 41-110 days in the freezer compartment of a refrigerator (−15°C) prior to insertion loss measurements.

2. Experiment 2: Additionally, the chest walls from six 6-to-7-week-old 19.2 ± 1.2-g female ICR mice and six 3-to-4-week-old 234 ± 6-g female rats were evaluated at various times postmortem to assess whether the long storage time affected attenuation coefficient estimates. The same six mouse chest walls were evaluated at 1, 22, and 144 days postmortem, and the same six rat chest walls were evaluated at 1, 22, 50, and 125 days postmortem. The chest walls were surgically removed as described above. Immediately following removal, the mouse and rat chest walls were placed in a 0.9% sodium chloride solution, sealed in Glad-Lock® Zipper™ sandwich bags, and stored in the freezer compartment of a refrigerator (−15°C) until insertion loss measurements were taken. These 12 animals were not part of the lung hemorrhage study.

B. Measurement and Analysis Techniques

Standard through-transmission insertion loss techniques were used [18] to estimate the attenuation coefficient of the chest wall intercostal space. Fig. 1 details the experimental set up. The source transducer was driven by either a Panametrics 5800 or Panametrics

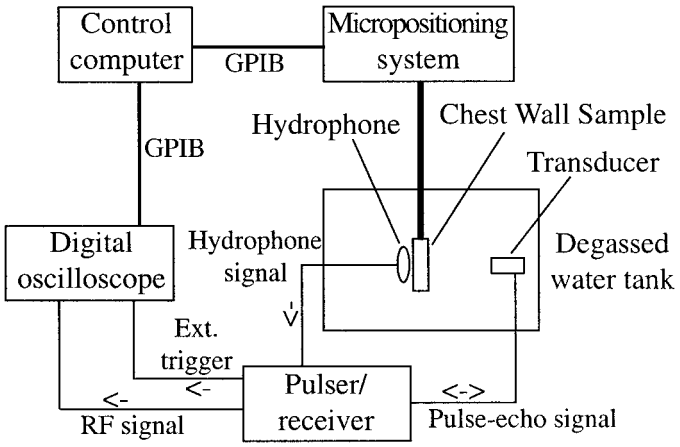

Fig. 1. Block diagram of measurement system that is used to estimate intercostal tissue attenuation coefficient.

5900 pulser/receiver (Panametrics, Waltham, MA). The pulser/receiver operated in both the pulse-echo mode and the through-transmission mode, and its 2-kHz pulse repetition frequency signal was fed to the source transducer. The source transducer was positioned rigidly in the water tank. The PVDF 1-mm^2 membrane hydrophone (either Perceptron Model 804, Plymouth Meeting, PA, or Marconi Model Y-34-3598, Chelmsford, England, UK) was mounted to a manually controlled three-axis positioning system (Daedal Inc., Harrison City, PA). All four of the source transducers were characterized prior to the experiments (see below), including their focal length. The hydrophone was positioned in the source's focal region by operating the pulser/receiver in its through-transmision mode, and monitoring the hydrophone's RF signal on the oscilloscope's time axis (6.5 μs/cm in water). The source transducer and hydrophone were oriented to maximize the PVDF hydrophone's receive signal amplitude without the sample in place by adjusting the position of both the source and hydrophone. The chest wall sample was mounted in a specially designed holder and positioned between the source transducer and the hydrophone, and as closely as possible to the hydrophone. The holder was mounted to a computer-controlled micropositioning system (Daedal Inc., Harrison City, PA) that has three orthogonal axes, each with a linear accuracy of 2 μm. The micropositioning system was controlled by the same computer that acquired the digitized pulse-echo and hydrophone signals from the oscilloscope (500 MS/s, LeCroy Model 9354TM, Chest-

nut Ridge, NY). The source transducer, the PVDF hydrophone, and the holder supporting the chest wall sample were immersed in 22°C degassed water.

Pulse-echo ultrasonic fields of each source transducer were characterized in degassed water (22°C) by an established technique [19]. Initially, two source transducers (transducers 1 and 2, see Table II) were used to cover the necessary frequency range of 2.5 to 6.5 MHz. However, because of their narrow bandwidth, two additional source transducers (transducers 3 and 4) were used, each with larger bandwidths that independently covered the necessary frequency range.

The mouse chest wall samples stored at 4°C (Experiment 1) were removed from the refrigerator and acclimated to room temperature for at least 10-20 minutes. The mouse and rat chest wall samples stored at −15°C (Experiments 1 and 2) were removed from the refrigerator and acclimated to room temperature for at least 30-60 minutes. For Experiment 2 chest wall samples, following each insertion loss measurements procedure, the chest wall samples were placed in a 0.9% sodium chloride solution, sealed in Glad-Lock® Zipper™ sandwich bags, and stored in the freezer compartment of a refrigerator (−15°C) until the next insertion loss measurements were taken.

No bubbles were visible on the chest wall samples because only the shaved and depiliated chest walls were used. If bubbles had been present, they would have shown up on the B-mode image (see below) that was used to assess sample thickness. Also, if some skin with hair still remaining was on the sample, the hair was removed prior to data acquisition.

The same measurement and analysis procedures were used for animals from both experiments. The chest wall sample was mounted to the specially designed holder on a laboratory workbench at room temperature after the sample had acclimatized to room temperature. The holder was then mounted to the computer-controlled micropositioning system, with the sample positioned between the source transducer and PVDF hydrophone in the tank's degassed water. The chest wall sample was placed in the tank's degassed water for at least 5 minutes for mice and 15 minutes for rats prior to taking measurements to ensure that it was acclimatized to the water's temperature (22°C). The sample was positioned with the chest wall's skin surface toward the source transducer, and with the skin surface approximately perpendicular to the transducer's beam axis. To facilitate data acquisition, the chest wall sample was oriented in the holder so that the sample could be moved perpendicular to the orientation of the ribs and to the ultrasound beam (note that the source transducer and PVDF hydrophone remain fixed spatially).

The sample was moved under computer control by the micropositioning system while the data were acquired. The length of the scan was selected to acquire data across at least four ribs so that acquired data included three intercostal spaces. The ribs provided spatial references for locating the intercostal tissue. The ultrasound beam intercepted the same tissue sample region twice: once with the pulser/receiver in pulse-echo mode and once with it in through-transmission mode. In this way, the through-transmission and pulse-echo data were acquired from the same tissue region. The through-transmission data were used for the insertion loss estimates, and the pulse-echo data were used to generate the B-mode image for tissue thickness and intercostal space measurements. For the mouse chest walls, data were acquired from 200 adjacent lateral positions over a 10-mm length in increments of 50 μm. For the rat chest walls, data were acquired from 400 adjacent lateral positions over a 20-mm length in increments of 50 μm. To acquire reference data, identical data acquisition procedures for the through-transmission mode were used, but with only degassed water between the source transducer and hydrophone. Reference data were acquired for each sample immediately following the acquisition of data from the chest wall sample. The digitized pulse-echo and through-transmission RF signals were transferred to a Sun UltraSparc workstation and analyzed using Matlab® (The Mathworks, Natick, MA).

The analysis program computed the Hilbert transform of the pulse-echo and through-transmission RF data of the chest wall sample. The transformed pulse-echo data were displayed as a conventional B-mode image. The transformed through-transmission data were peak detected for each scan position and displayed as a through-transmission (normalized) acoustic pressure profile (Fig. 2). These two displays were used to locate the intercostal tissue in the data base. The ribs were clearly seen in the B-mode image, and the normalized acoustic pressure profile (Fig. 2) demonstrated a substantial amplitude decrease through the region in which the ribs were located. Sample thickness in the region of the intercostal tissue was estimated from the B-mode image by assuming 1540 m/s as the speed of sound. The through-transmission RF waveforms corresponding to the intercostal spaces were kept in a reduced matrix for further processing.

All of the reference (water path) through-transmission RF data was read in next. The FFT of each water-path signal was taken, and then the power spectrum was calculated. The average of the power spectra for all the water-path signals was calculated to give the reference spectrum. Next, the FFT and power spectra of the through-transmission RF waveforms corresponding to the intercostal spaces (the reduced matrix) were calculated. The power spectra of all of these sample waveforms were averaged. The insertion loss (in dB) was found from the reference and sample spectra for a range of frequencies within the bandwidth of the transducer. The insertion loss was divided by the thickness of the sample, as calculated previously from the pulse-echo data, to yield the attenuation coefficient (in dB/cm).

C. Microscopic Measurement of Layers of the Intercostal Tissue

Intact chest walls were obtained from mice and rats immediately following euthanasia. The chest walls were

TABLE II
MEASURED CHARACTERISTICS OF THE FOUR 19-MM-DIAMETER FOCUSED SOURCE TRANSDUCERS USED TO ESTIMATE INTERCOSTAL TISSUE ATTENUATION COEFFICIENT.

Transducer number*	Center frequency (MHz)	−3-dB fractional bandwidth (%)	Focal length (mm)	−6-dB beamwidth at focus (μm)	−6-dB depth of focus (mm)
1 (98C157)	2.83	7.93	20.1	239	2.18
2 (98C153)	5.53	11.0	42.5	521	6.51
3 (262277)	4.03	32.7	84.0	1300	15.9
4 (68655)	7.18	43.5	50.7	556	9.41

*Transducers 1 and 2: Valpey Fisher (Hopkinton, MA). Transducers 3 and 4: Panametrics, Inc. (Waltham, MA).

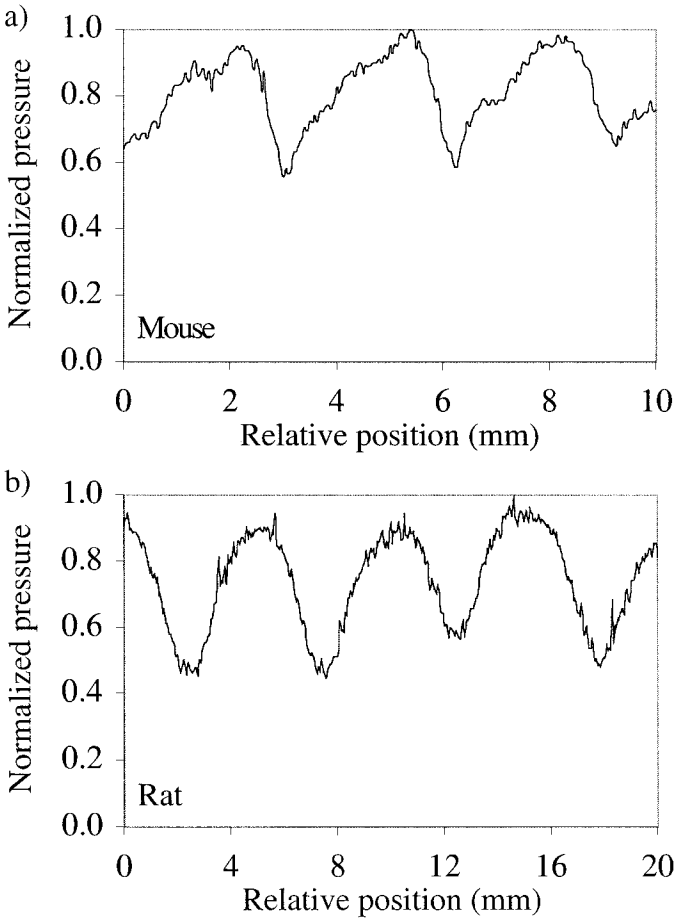

Fig. 2. Typical through-transmission (normalized) acoustic pressure profiles as a function of lateral scanned position for (a) mice and (b) rats from which the intercostal (between the ribs) tissue location (maximum acoustic pressure values) is identified, and the attenuation coefficient of the intercostal tissue is estimated. The location of the ribs is at the minimum acoustic pressure values.

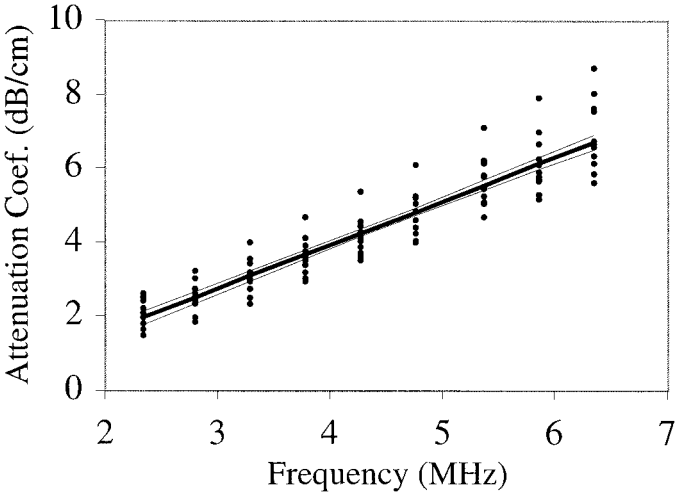

Fig. 3. Intercostal tissue attenuation coefficient as a function of frequency for 13 of the 27 rats from Experiment 1 using Transducer 3 (center frequency: 4.03 MHz). The individual data points represent the frequency-dependent attenuation coefficients between 2.3 and 6.3 MHz in 0.5-MHz increments for each of the 13 intercostal tissue sets. The thicker line represents the regression expression, and the thinner lines represent the ±95% confidence limits.

fixed by immersion in 10% neutral-buffered formalin, processed, embedded in paraffin, sectioned at 5 μm, stained with hematoxylin and eosin, and evaluated with light microscopy. Chest walls were embedded in paraffin with an orientation such that histologic sections were cut at right angles to the ribs through four to five ribs. The tissue between the ribs (intercostal tissue: skin, panniculus muscle, subcutaneous adipose tissue [fat], and intercostal muscle) from the skin surface to the parietal pleura was used for measurements. A digital image of each intercostal tissue area was obtained using a Nikon Optiphot-2 microscope equipped with a 4× objective and a Sony color video camera. In addition, a digital image of a slide micrometer (2-mm total length divided into units of 0.01 mm) was obtained with a 4× objective using the same microscopy system. Using Adobe Photoshop (Adobe, San Jose, CA), the digital image of intercostal tissue for each mouse and rat was overlaid with the digital image of the slide micrometer. The thickness measurements of each tissue layer in the intercostal space were determined in each animal using this procedure.

III. RESULTS

A. Experiments

1. Experiment 1: Fig. 3 shows a typical analyzed intercostal tissue attenuation coefficient data set for 13 of the 27 rats from Experiment 1 using Transducer 3. The individual data points represent intercostal tissue attenuation coefficients between 2.3 and 6.3 MHz in 0.5-MHz increments (or nine values per tissue sample) for each of the

13 data sets, that is, at each of the nine frequencies, there are 13 attenuation coefficient values. The linear regression analysis of this data set (n = 13 × 9 = 117) yields a regression equation along with the ±95% confidence limits.

Graphical representation of the frequency-dependent regression analyses is shown in Fig. 4 for the intercostal tissue from the chest walls of 41 mice and 27 rats. The linear regression equations for the four curves (Fig. 4) are:

A = 1.29f − 0.70 14 mice frequency range: 1.8–3.8 MHz
r^2 = 0.37, SER = 0.50, SES = 0.084
A = 0.89f + 0.91 27 mice frequency range: 4.6–7.1 MHz
r^2 = 0.19, SER = 1.5, SES = 0.13
A = 1.18f − 0.79 13 rats frequency range: 2.3–6.3 MHz
r^2 = 0.88, SER = 0.58, SES = 0.041
A = 1.30f − 1.29 14 rats frequency range: 3.2–8.2 MHz
r^2 = 0.81, SER = 1.0, SES = 0.041

where the attenuation coefficient (A) is in decibel per centimeter and the ultrasonic frequency (f) is in megahertz. The regression analysis [20] yielded the coefficient of determination, r^2, the standard error of regression, SER, and the standard error of the slope term, SES. It is common to see the attenuation coefficient normalized to frequency (in dB/cm-MHz), which is the slope term for these regressions, to which the SES applies.

A power law fit that combined the intercostal tissue data from the 41 mice and 27 rats yielded $A = 0.89\,f^{1.1}$.

2. Experiment 2: Independently, the same six mouse chest wall samples were evaluated at three time points (1, 22, and 144 days postmortem) and the same six rat chest wall samples were evaluated at four time points (1, 22, 50, and 125 days postmortem) to determine if there was an effect of storage time on the intercostal tissue attenuation coefficient. These chest wall samples were not included in Experiment 1. Graphical representation of the frequency-dependent regression analyses for intercostal tissue is shown in Fig. 5. The linear regression equations for the seven curves (Fig. 5) are:

A = 1.54f − 0.71 mouse 1 day pm frequency range: 3.7–8.2 MHz
r^2 = 0.76, SER = 1.4, SES = 0.12
A = 1.28f + 1.28 mouse 22 days pm frequency range: 3.7–8.2 MHz
r^2 = 0.75, SER = 1.2, SES = 0.10
A = 1.54f − 0.44 mouse 144 days pm frequency range: 3.7–8.2 MHz
r^2 = 0.74, SER = 1.4, SES = 0.12
A = 1.15f − 0.91 rat 1 day pm frequency range: 3.7–8.2 MHz
r^2 = 0.86, SER = 0.75, SES = 0.058
A = 1.01f − 0.023 rat 22 days pm frequency range: 3.7–8.2 MHz
r^2 = 0.76, SER = 0.92, SES = 0.071
A = 1.12f − 0.93 rat 50 days pm frequency range: 3.7–8.2 MHz
r^2 = 0.84, SER = 0.80, SES = 0.062
A = 0.99f − 0.12 rat 125 days pm frequency range: 3.7–8.2 MHz
r^2 = 0.45, SER = 1.8, SES = 0.14

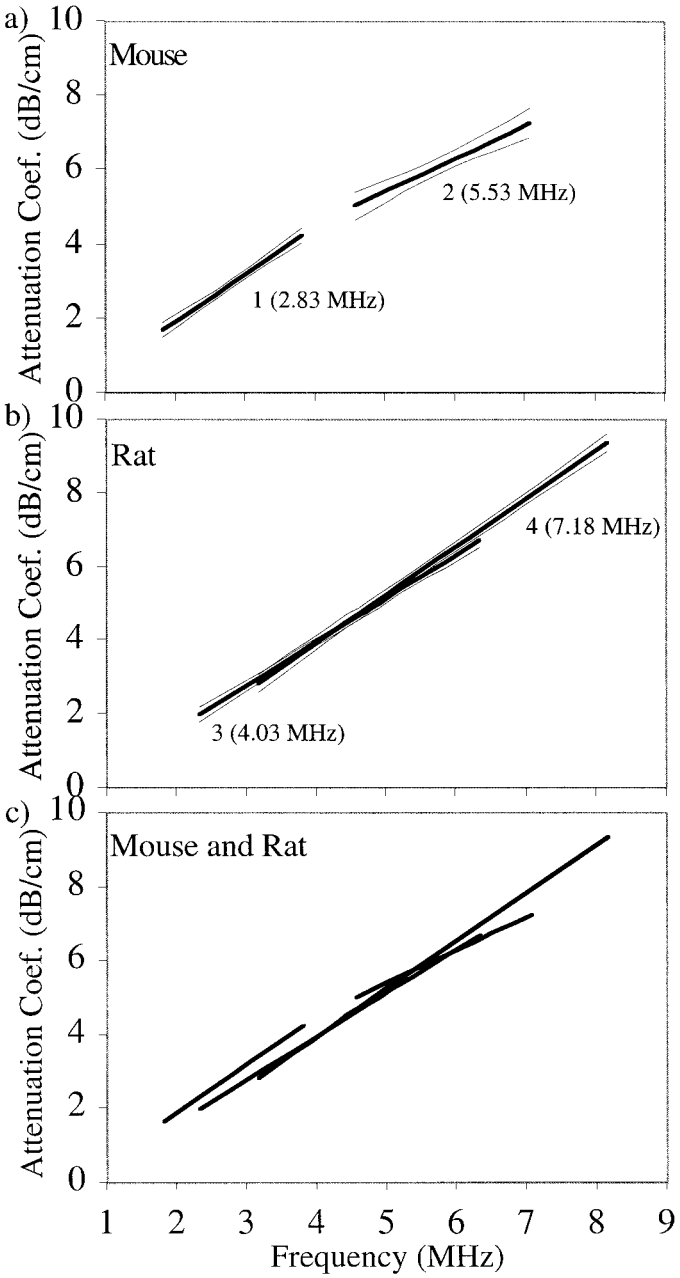

Fig. 4. Regression analysis (linear regression line ±95% confidence limits) of intercostal tissue attenuation coefficient as a function of frequency for the chest walls of (a) 41 mice, (b) 27 rats from Experiment 1. The thicker lines represent the regression expressions, and the thinner lines represent the ±95% confidence limits. The numbers in (a) and (b) represent the source transducer number (center frequency) (see Table II). (c) Only the four regression lines from (a) and (b) are plotted.

B. Summary

Fig. 6 shows all 11 intercostal tissue attenuation coefficient regression equations (without the 95% confidence

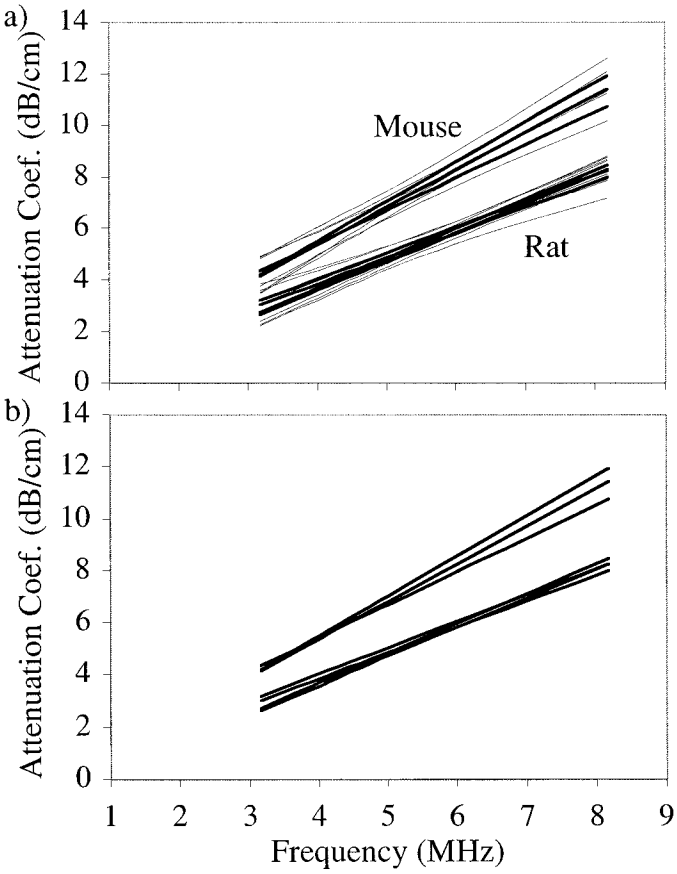

Fig. 5. (a) Regression analyses (linear regression line ±95% confidence limits) of intercostal tissue attenuation coefficient as a function of frequency for the chest walls of six mice at days 1, 22, and 144 postmortem (top three regressions) and of six rats at days 1, 22, 50, and 125 postmortem (bottom four regressions) from Experiment 2. The thicker lines represent the regression expressions, and the thinner lines represent the ±95% confidence limits. Transducer 4 (7.18 MHz) is the source transducer (see Table II). (b) Only the seven regression lines from (a) are plotted.

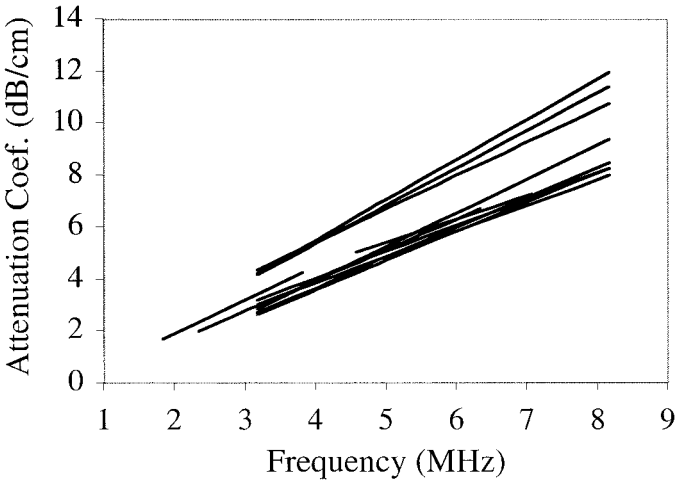

Fig. 6. All eleven intercostal tissue attenuation coefficient regression equations (without the 95% confidence limits) as a function of frequency (Experiments 1 and 2 combined). The three regression equations that are not grouped with the other eight are from the timed mouse study (Experiment 2).

limits) listed above for ease of direct comparisons. Eight of the regressions are essentially overlapping, and the three regressions from the timed mouse study (Experiment 2, see Fig. 5) have a slightly greater attenuation coefficient. The eight regression equations that are grouped together are not individually labeled in order to demonstrate their similarity.

IV. Discussion

There is excellent agreement between the mouse and rat intercostal tissue attenuation coefficients as a function of frequency. The only exception is the mouse time studies (Fig. 5, Experiment 2) at 1, 22, and 144 days postmortem, although there is excellent agreement among these three time points. These six mice were much smaller than the 41 mice evaluated at day 1 postmortem [Fig. 4(a), Experiment 1], that is, 19.2 ± 1.0 g compared to 34.3 ± 6.4 g. The smaller size did not affect the center-to-center rib spacing (about 3 mm for all mice). Thus, the intercostal tissue attenuation coefficient difference may be attributed to the tissue of the intercostal space, or to a greater uncertainty in estimating the intercostal tissue thicknesses (mean±SD thickness for the 41 larger mice is 4.9 ± 0.8 mm, and for the 6 smaller mice it is 2.6 ± 0.4 mm).

Another possible explanation for the intercostal tissue attenuation coefficient differences in the two mouse experiments might be attributed to sample handling. The chest walls from the 41 larger mice (Experiment 1) were the only samples that were not frozen.

Nonetheless, a very important finding in this study is that the temporal studies (Fig. 5) clearly show that the time postmortem does not affect the attenuation coefficient estimates in either mice or rats, although there is a difference between the mice and rats intercostal tissue attenuation coefficients. This finding provides support for estimating the intercostal tissue attenuation coefficients at day one postmortem from attenuation coefficient estimates at various times postmortem. In other words, sample storage did not appear to affect the intercostal tissue attenuation coefficient.

The rats from both experiments had the same center-to-center rib spacing (5 mm). Also, rats from both experiments had about the same chest wall thickness (mean±SD thickness for the 26 larger rats used in the lung study was 7.9 ± 0.8 mm, and for the 6 smaller rats used for the time study it was 7.2 ± 0.9 mm). The rat chest walls were similarly stored. Thus, these similarities may account for the attenuation coefficient agreement between the two rat experiments.

The attenuation coefficient measurements were conducted at a temperature of 22°C. Our purpose was to estimate the intercostal tissue attenuation coefficient of the mice and rats used in the ultrasound-induced lung hemorrhage study so that the in-situ (at the pleural surface) ultrasonic exposure levels could be estimated. For the

lung hemorrhage studies, the anesthetized animals were placed in degassed 30°C water. The sparse temperature-dependent attenuation coefficient literature was evaluated to estimate the temperature dependency of the intercostal tissue, but no reports could be found for intercostal tissue. Because intercostal tissue is composed of different tissue types (skin, panniculus muscle, subcutaneous adipose tissue [fat], intercostal muscle), the fraction of each of these tissue types was histologically evaluated for four mice and two rats. Mice and rats, respectively, have the following percentages (mean±SD): $19 \pm 4.7\%$ and $27 \pm 2.7\%$ for skin, $8.4 \pm 3.8\%$ and $11 \pm 2.5\%$ for panniculus muscle, $13 \pm 8.6\%$ and $12 \pm 4.5\%$ for subcutaneous adipose tissue [fat], $60 \pm 9.2\%$ and $50 \pm 6.7\%$ for intercostal muscle.

Fat has a relatively strong but highly variable temperature-dependent attenuation coefficient, ranging between -0.08 and -0.2 dB/cm/°C for porcine back fat, and between $+0.09$ and -0.6 dB/cm/°C for bovine peritoneal fat [21]. Muscle has a weak temperature-dependent attenuation coefficient, ranging between -0.006 dB/cm/°C for canine heart muscle [22] and $+0.04$ dB/cm/°C for bovine skeletal muscle [23]. No reports could be found for skin, but generally the temperature-dependent attenuation coefficient for most soft tissues is in the range of those just reported [24]. Because the vast majority of intercostal tissue is nonfat soft tissue, it is assumed that there is a negligible change in the attenuation coefficient over the relatively narrow temperature range between 22 and 30°C.

Mouse chest wall attenuation reported in [1] ranged between 1.5 and 5.2 dB at a frequency of 1.1 MHz, and between 2.5 and 6.9 dB at a frequency of 3.4 MHz. Also, [4] used a mouse chest wall attenuation of 1.9 dB at a frequency of 1.1 MHz. At the 3.4-MHz frequency, our mouse attenuation was estimated to be between 1.8 and 1.9 dB, using a chest wall thickness of 4.9 mm. Extrapolating our results to a frequency of 1.1 MHz, our mouse attenuation was estimated to be at least a factor of two lower, that is, between 0.4 and 0.9 dB, using a chest wall thickness of 4.9 mm. In general, our values for the mouse are a bit lower than those determined by others [1], [4]. Attenuation or insertion loss values for the rat have not been reported previously.

As a general rule, the frequency normalized attenuation coefficient for intercostal tissue of adult mice and rats can be adequately described numerically by 1.1 dB/cm-MHz.

Acknowledgments

We thank Dr. C. Frazier for assistance in developing the analysis programs, and D. Abano, R. Bashyal, J. Blue, J. Brown, J. Christoff, B. McNeill, K. Norrell, and S. Talwalker for their technical contributions.

References

[1] S. Z. Child, C. L. Hartman, L. A. Schery, and E. L. Carstensen, "Lung damage from exposure to pulsed ultrasound," *Ultrasound Med. Biol.*, vol. 16, pp. 817–825, 1990.

[2] C. Hartman, S. Z. Child, R. Mayer, E. Schenk, and E. L. Carstensen, "Lung damage from exposure to the fields of an electrohydraulic lithotripter," *Ultrasound Med. Biol.*, vol. 16, pp. 675–679, 1990.

[3] D. P. Penney, E. A. Schenk, K. Maltby, C. Hartman-Raeman, S. Z. Child, and E. L. Carstensen, "Morphologic effects of pulsed ultrasound in the lung," *Ultrasound Med. Biol.*, vol. 19, pp. 127–135, 1993.

[4] C. H. Raeman, S. Z. Child, and E. L. Carstensen, "Timing of exposures in ultrasonic hemorrhage of murine lung," *Ultrasound Med. Biol.*, vol. 19, pp. 507–517, 1993.

[5] L. A. Frizzell, E. Chen, and C. Lee, "Effects of pulsed ultrasound on the mouse neonate: Hind limb paralysis and lung hemorrhage," *Ultrasound Med. Biol.*, vol. 20, pp. 53–63, 1994.

[6] J. F. Zachary and W. D. O'Brien, Jr., "Lung lesion induced by continuous- and pulsed-wave (diagnostic) ultrasound in mice, rabbits, and pigs," *Vet. Pathol.*, vol. 32, pp. 43–54, 1995.

[7] C. H. Raeman, S. Z. Child, D. Dalecki, C. Cox, and E. L. Carstensen, "Exposure-time dependence of the threshold for ultrasonically induced murine lung hemorrhage," *Ultrasound Med. Biol.*, vol. 22, pp. 139–141, 1996.

[8] W. D. O'Brien, Jr. and J. F. Zachary, "Lung damage assessment from exposure to pulsed-wave ultrasound in the rabbit, mouse, and pig," *IEEE Trans. Ultrason., Ferroelect., Freq. Contr.*, vol. 44, pp. 473–485, 1997.

[9] D. Dalecki, S. Z. Child, C. H. Raeman, D. P. Penney, C. Cox, D. P. Penny, and E. L. Carstensen, "Age dependence of ultrasonically induced lung hemorrhage in mice," *Ultrasound Med. Biol.*, vol. 23, pp. 767–776, 1997.

[10] C. K. Holland, K. Sandstrom, X. Zheng, J. Rodriguey, and R. A. Roy, "The acoustic field of a pulsed Doppler diagnostic ultrasound system near a pressure-release surface," *J. Acoust. Soc. Amer.*, vol. 95, p. 2855, 1994 (abstract).

[11] C. K. Holland, C. X. Deng, R. E. Apfel, J. L. Alderman, L. A. Ferandez, and K.J.W. Taylor, "Direct evidence of cavitation in vivo from diagnostic ultrasound," *Ultrasound Med. Biol.*, vol. 22, pp. 917–925, 1996.

[12] A. F. Tarantal and D. R. Canfield, "Ultrasound-induced lung hemorrhage in the monkey," *Ultrasound Med. Biol.*, vol. 20, pp. 65–72, 1994.

[13] R. Baggs, D. P. Penney, C. Cox, S. Z. Child, C. H. Raeman, D. Dalecki, and E. L. Carstensen, "Thresholds for ultrasonically induced lung hemorrhage in neonatal swine," *Ultrasound Med. Biol.*, vol. 22, pp. 119–128, 1996.

[14] D. Dalecki, S. Z. Child, C. H. Raeman, C. Cox, and E. L. Carstensen, "Ultrasonically induced lung hemorrhage in young swine," *Ultrasound Med. Biol.*, vol. 23, pp. 777–781, 1997.

[15] W. D. O'Brien, Jr., L. A. Frizzell, R. M. Weigel, and J. F. Zachary, "Ultrasound-induced lung hemorrhage is not caused by inertial cavitation," *J. Acoust. Soc. Amer.*, vol. 108, pp. 1290–1297, 2000.

[16] J. F. Zachary, J. M. Sempsrott, L. A. Frizzell, D. G. Simpson, and W. D. O'Brien, Jr., "Superthreshold behavior and threshold estimation of ultrasound-induced lung hemorrhage in adult mice and rats," *IEEE Trans. Ultrason., Ferroelect., Freq. Contr.*, vol. 48, no. 2, pp. 581–592, Mar. 2001.

[17] *Mechanical Bioeffects from Diagnostic Ultrasound: AIUM Consensus Statements*, American Institute of Ultrasound in Medicine, Laurel, MD, 1998.

[18] E. L. Madsen, F. Dong, G. R. Frank, B. S. Gara, K. A. Wear, T. Wilson, J. A. Zagzebski, H. L. Miller, K. K. Shung, S. H. Wang, E. J. Feleppa, T. Liu, W. D. O'Brien, Jr., K. A. Topp, N. T. Sanghvi, A. V. Zaitsen, T. J. Hall, J. B. Fowlkes, O. D. Kripfgans, and J. G. Miller, "Interlaboratory comparison of ultrasonic backscatter, attenuation and speed measurements," *Ultrasound Med. Biol.*, vol. 18, pp. 615–631, 1999.

[19] K. Raum and W. D. O'Brien, Jr., "Pulse-echo field distribution measurement technique of high-frequency ultrasound sources," *IEEE Trans. Ultrason., Ferroelect., Freq. Contr.*, vol. 44, pp. 810–815, 1997.

[20] S. Weisberg, *Applied Linear Regression*. New York: Wiley, 1980.

[21] M. J. Haney and W. D. O'Brien, Jr., "Temperature dependency of ultrasonic propagation properties in biological materials," in *Tissue Characterization with Ultrasound*. vol. I, J. F. Greenleaf, Ed. Boca Raton, FL: CRC Press, Inc., 1986, pp. 15–55.

[22] M. O'Donnell, J. W. Mimbs, B. E. Sobel, and J. G. Miller, "Ultrasonic attenuation of myocardial tissue: Dependence on time after excision and on temperature," *J. Acoust. Soc. Amer.*, vol. 62, pp. 1054–1057, 1977.
[23] N. B. Smith, "Effect of myofibril length and tissue constituents on acoustic propagation properties of muscle," Ph.D. dissertation, University of Illinois, Urbana, IL, 1996.
[24] F. A. Duck, *Physical Properties of Tissue. A Comprehensive Reference Book*. New York: Academic Press, 1990.

Geraldine A. Teotico was born on August 31, 1976, in Chicago, IL. She graduated with a B.S. degree in bioengineering from the University of Illinois, Urbana-Champaign in 1998 and was awarded high distinction for her senior thesis on "Dependency of Attenuation, Propagation Speed and Backscatter on Fixed Skeletal Muscle Fiber Orientation".

She was employed by the University of Illinois, Urbana-Champaign, Department of Electrical and Computer Engineering from June 1998 to June 1999 as a visiting scholar and contributed to research on bioeffects of ultrasound on lung tissue. Since January 2000 she has been employed by Crowe Chizek and Company, LLP, as a systems integration consultant.

Rita J. Miller was born in San Diego, California. She received her D.V.M at the University of Wisconsin, Madison in 1992.

Dr. Miller completed a small animal medical/surgical internship at the University of Illinois at Urbana-Champaign in 1993. She then worked as a Veterinary Poison Information Specialist at the National Animal Poison Control Center, also at the University of Illinois at Urbana-Champaign. While at the University of Illinois she has been involved with a variety of research projects. Evaluation of the efficacy of a new treatment for Erlichiosis in dogs. Rehabilitation with electrical muscle stimulation for dogs with surgically treated cranial cruciate ligament deficient stifles. Role of IGF-1 (insulin-like growth factor 1) and the IGF-1R (type one insulin-like growth factor one receptor) in the uterotrophic effect induced by the administration of tamoxifen. Identification and cloning of canine MMP-2 (matrix metalloproteinase-2). RT-PCR (reverse-transcription polymerase chain reaction) profiling of canine spontaneous tumors for the presence of MMP-2. Her current research involves the assessment of ultrasound-induced lung damage and attenuation coefficient determination of intercostal tissues.

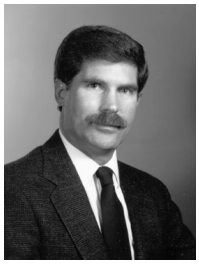

Leon A. Frizzell (S'71–M'74–SM'82) was born in West Stewartstown, NH, on September 12, 1947. He received the B.S. degree in physics from the University of New Hampshire, Durham, in 1969, and the M.S. and Ph.D. degrees in electrical engineering from the University of Rochester, Rochester, NY, in 1971 and 1976, respectively.

Since 1975, he has been in the Department of Electrical and Computer Engineering at the University of Illinois at Urbana-Champaign, where he is currently a professor of electrical and computer engineering and bioengineering. He was Acting Director of the Bioacoustics Research Laboratory within the Department of Electrical and Computer Engineering from August 1989 to August 1990 and served as Chair of the Bioengineering Faculty from August 1995 to December 1999. He was also a visiting research scientist at Yale University from August 1985 to August 1986. His research interest are in ultrasound and include tissue characterization, biological effects, hyperthermia, surgery, and bioengineering.

Dr. Frizzell is a Fellow of the American Institute of Ultrasound in Medicine, Fellow of the Acoustical Society of America, Fellow of the American Institute for Medical and Biological Engineering, and a member of Eta Kappa Nu and Sigma Xi.

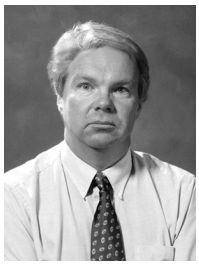

James F. Zachary received a B.S. degree from Northern Illinois University, Dekalb, in 1972 and D.V.M. and Ph.D. degrees in 1977 and 1983, from the University of Illinois, Urbana-Champaign.

From 1978, he has been at the University of Illinois, where he is an Associate Professor of Pathology. His research interests involve ultrasound-tissue interaction and include biological effects, tissue characterization, blood-flow measurements, and acoustic microscopy. He also studies the role of microglial cells, astrocytes, and brain cytokines in neurodegenerative diseases. He has published more than 50 papers.

Dr. Zachary is Editor-in-Chief of *Veterinary Pathology*. He is a Diplomate in the American College of Veterinary Pathologists and a member of the American Institute of Ultrasound in Medicine (AIUM) and its Bioeffects Committee, the American Society for Investigative Pathology (FASEB), and the Society for Neuroscience.

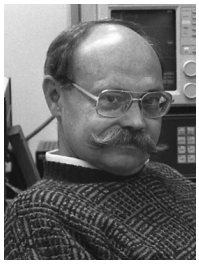

William D. O'Brien, Jr. (S'64–M'70–SM'79–F'89) received the B.S., M.S., and Ph.D. degrees in 1966, 1968, and 1970, from the University of Illinois, Urbana-Champaign.

From 1971 to 1975 he worked with the Bureau of Radiological Health (currently the Center for Devices and Radiological Health) of the U.S. Food and Drug Administration. Since 1975, he has been at the University of Illinois, where he is a professor of electrical and computer engineering and bioengineering, College of Engineering; professor of Bioengineering, College of Medicine; professor of Nutritional Sciences, College of Agricultural, Consumer and Environmental Sciences; a research professor in the Beckman Institute for Advanced Science and Technology; and a research professor in the Coordinated Science Laboratory. He is the Director of the Bioacoustics Research Laboratory. He also is the program director of the NIH Radiation Biophysics and Bioengineering in Oncology Training Program. His research interests involve the many areas of ultrasound-tissue interaction, including spectroscopy, risk assessment, biological effects, tissue characterization, dosimetry, blood-flow measurements, acoustic microscopy, and imaging, for which he has published 215 papers.

Dr. O'Brien is Editor-in-Chief of the *IEEE Transactions on Ultrasonics, Ferroelectrics, and Frequency Control*. He is a Fellow of the

Institute of Electrical and Electronics Engineers (IEEE), the Acoustical Society of America (ASA), a Fellow of the American Institute of Ultrasound in Medicine (AIUM), and a Founding Fellow of the American Institute of Medical and Biological Engineering. He was recipient of the IEEE Centennial Medal (1984), the AIUM Presidential Recognition Awards (1985 and 1992), the AIUM/WFUMB Pioneer Award (1988), the IEEE Outstanding Student Branch Counselor Award for Region 4 (1989), the AIUM Joseph H. Holmes Basic Science Pioneer Award (1993), and the IEEE Ultrasonics, Ferroelectrics, and Frequency Control Society Distinguished Lecturer (1997-1998). He received the IEEE Ultrasonics, Ferroelectrics, and Frequency Control Society's Achievement Award for 1998, and the IEEE Millennium Medal in 2000. He has served as Co-Chair of the 1981 IEEE Ultrasonic Symposium, General Chair of the 1988 IEEE Ultrasonics Symposium. He is Co-Chair of both the 2001 and 2003 IEEE Ultrasonics Symposia. He has been Secretary-Treasurer (1972-1980), Vice President (1981), and President (1982-1983) of the IEEE Sonics and Ultrasonics Group (currently the IEEE Ultrasonics, Ferroelectrics, and Frequency Control Society). He has been Treasurer (1982-1985), President-Elect (1986-1988), and President (1988-1991) of the American Institute of Ultrasound in Medicine. He has served on the Board of Directors (1988-1993) of the American Registry of Diagnostic Medical Sonographers, and he was Treasurer (1991-1994) of the World Federation for Ultrasound in Medicine and Biology.